Applied Physics A (2021) 127:313
https://doi.org/10.1007/s00339-021-04453-5

Applied Physics A
Materials Science & Processing

Thermally induced transitions and depolarization of Fe_2O_3 doped PMnS-PZN-PZT piezoelectric ceramics

Huazhang Zhang[1,2] · Jing Zhou[1] · Jie Shen[1] · Jingjing Zhou[1] · Zhi Wu[3] · Daping He[1,2] · Wen Chen[1]

Received: 16 January 2021 / Accepted: 19 March 2021 / Published online: 5 April 2021

Abstract

Thermally induced transitions and depolarization of Fe_2O_3 doped PMnS-PZN-PZT ceramics are investigated. The ceramics have a highly diffused dielectric peak, but the temperature for the maximum dielectric permittivity T_m is frequency independent, which rules out the ceramics to be classified as typical relaxors. Meanwhile, the depolarization temperature T_d determined by the thermally stimulated depolarization current is found to be notably lower than T_m, which is distinct from the behaviors of normal ferroelectrics as well. An extraordinary phenomenon noted is that the T_d coincides quite well with a characteristic temperature where the dielectric permittivity shows the fastest increase. This characteristic temperature, denoted as $T_{F\text{-}R}$, is faint in the temperature-dependent dielectric permittivity but can be well resolved by taking the first derivative of dielectric permittivity with respect to temperature. In addition, it is found a number of features of the anomaly around $T_{F\text{-}R}$ that are quite similar to the ferroelectric-to-relaxor transition in typical relaxors, and therefore, the $T_{F\text{-}R}$ is assigned to a transition from ferroelectric state to a "relaxor-like" state, in which the correlation of ferroelectric order could be weakened. Complex impedance analysis reveals the presence of small polarizable entities at high temperature, providing further support for the high-temperature relaxor-like state. It is suggested that the depolarization of Fe_2O_3 doped PMnS-PZN-PZT is related to the disruption of long-range ferroelectric order into polar regions with small sizes, rather than the ferroelectric-to-paraelectric transition.

Keywords PMnS-PZN-PZT ceramics · Depolarization · Ferroelectric transition · Relaxor ferroelectrics

1 Introduction

Thermal depolarization of ferroelectrics refers to the phenomenon that the remanent polarization and piezoelectricity degrade at elevated temperatures [1–3]. The depolarization temperature T_d is one of the most important issues for piezoelectric applications, because it determines the upper temperature limit for the use of piezoelectric materials [4–9]. Particularly, for the high-power piezoelectric applications, such as piezoelectric transducers, ultrasonic motors, etc., where the piezoelectric ceramics are operated at vibration modes of high velocities, the thermal stability of piezoelectric property and the related depolarization phenomenon are of critical importance. A significant concern is that the heat generation caused by the ceramic losses may lead to temperature rising, and, if the temperature excesses the depolarization temperature, it may consequently result in device failure [10–14]. In this context, understanding the depolarization behavior is imperative, which provides the basis for not only device applications but also performance improvement in piezoelectric ceramics.

Extensive research works have been devoted into the depolarization issue. It has been found that the depolarization process varies for different types of ferroelectrics. Normal ferroelectrics are expected to be depolarized in the vicinity of the Curie temperature T_C, along with the ferroelectric-to-paraelectric transition [1]. Besides, the thermally

✉ Wen Chen
chenw@whut.edu.cn

[1] State Key Laboratory of Advanced Technology for Materials Synthesis and Processing, School of Materials Science and Engineering, Wuhan University of Technology, Wuhan 430070, People's Republic of China

[2] Hubei Engineering Research Center of RF-Microwave Technology and Application, School of Science, Wuhan University of Technology, Wuhan 430070, People's Republic of China

[3] School of Materials and Chemistry Engineering, Hunan Institute of Technology, Hengyang 421002, People's Republic of China

activated reorientation of ferroelectric domains may also cause the decrease of remanent polarization and piezoelectric properties below T_C [15, 16]. Relaxor ferroelectrics are characterized by diffused dielectric peak, with pronounced frequency dispersion in the temperature of maximum dielectric constant T_m, i.e., the T_m shifts to higher temperatures with the increase of measurement frequency [17]. The relaxor ferroelectrics usually have a depolarization temperature T_d well below T_m [18–20]. It is generally accepted that in relaxor ferroelectrics the T_m does not correspond to any phase transitions, whereas the T_d is usually associated with the transition from the electric field-induced ferroelectric state to the high-temperature relaxor state [19, 21, 22]. Different from the ferroelectric-to-paraelectric transition, where the crystal losses the spontaneous polarization on both macroscopic and microscopic scales, the ferroelectric-to-relaxor transition is merely a macrodomain-to-microdomain transition, i.e., the macroscopic polarization fades away with the disruption of long-range ferroelectric order, whereas the microscopic spontaneous polarization still persists locally within the so-called polar nanoregions (PNRs) [17]. In the crossover from normal to relaxor ferroelectrics, there is another kind of ferroelectrics with intermediate electrical behavior, i.e., the dielectric peak is highly diffused, but the temperature of the dielectric maximum does not change with frequency. At present, only a few studies focus on the depolarization of this kind of ferroelectrics [23]. It still remains unclear whether their depolarization process is similar to that of the normal ferroelectrics or relaxor ferroelectrics, or there may be a completely different depolarization process in this kind of ferroelectrics.

Fe_2O_3 doped quaternary solid-solution $Pb(Mn_{1/3}Sb_{2/3})O_3$-$Pb(Zn_{1/3}Nb_{2/3})O_3$-$PbZrO_3$-$PbTiO_3$ (PMnS-PZN-PZT) ceramics are promising for high-power piezoelectric applications. The ceramics possess relatively large piezoelectric properties (piezoelectric constant $d_{33} = 356$ pC/N, planar electromechanical coupling coefficient $k_p = 0.60$) and simultaneously low losses (dielectric loss factor tan $\delta = 0.12\%$, mechanical quality factor $Q_m = 745$) [24]. To facilitate practical applications, a comprehensive understanding of the ceramic properties is required. Previously, we have measured the complete set of elastic, dielectric and piezoelectric parameters and characterized the high-field nonlinear properties as well [25, 26]. Nevertheless, the thermally induced transitions and the depolarization behavior of the ceramics are still remained to be clarified. In addition, the Fe_2O_3 doped PMnS-PZN-PZT is among the ceramics that exhibit diffused dielectric peak but no frequency dispersion in dielectric maximum temperature (see Sec. 3.2). Therefore, the investigations on Fe_2O_3 doped PMnS-PZN-PZT ceramics may also have an implication for understanding the thermal depolarization of ferroelectrics with behaviors intermediate between normal and relaxor ferroelectrics. By the above considerations, we herein perform the investigations on the thermally induced transitions and depolarization of the Fe_2O_3 doped PMnS-PZN-PZT ceramics.

2 Experimental

The 0.45 wt.% Fe_2O_3 doped PMnS-PZN-PZT ceramics were synthesized via conventional solid-state route. According to our previous works, the base material PMnS-PZN-PZT belongs to the morphotropic phase boundary (MPB) region, in which the tetragonal and rhombohedral phases are coexisted, and Fe_2O_3 is chosen as the dopant because it is an acceptor, which can effectively lower the losses [24, 27–29]. Analytical grade Pb_3O_4, MnO_2, Sb_2O_3, ZnO, Nb_2O_5, ZrO_2, TiO_2 and Fe_2O_3 powders were used as starting materials. The calcination was conducted at 900 °C for 2 h, and the sintering was conducted at 1280 °C for 2 h. During the sintering process, Pb-rich atmosphere was applied to minimize the lead loss. The sintered ceramics were polished and then electroded with silver paste. The poling procedure was conducted by applying a DC field of 3.0 kV/mm for 15 min at 150 °C in silicone oil bath.

The micromorphology of the ceramics was observed using a scanning electron microscope (FESEM, Ultra Plus-43–13, Zeiss, Germany). The crystal structure was examined using an X-ray diffractometer (XRD, PANalytical X'Pert Pro, Philips, Netherlands) with CuKα radiation. Rietveld refinement of the XRD patterns was performed using the program Maud [30]. For electrical measurements, the temperature-dependent dielectric properties and impedance spectra were measured by an LCR meter (TH2818, Tonghui Technologies Inc., China) connected to a computer-controlled furnace. The temperature-dependent dielectric properties are measured at a heating or cooling rate of 2 °C/min. The thermally stimulated depolarization current (TSDC) was measured using an amperemeter (Keithley 2430, Keithley Instruments Inc., America) connected to the same furnace at the same heating rate of 2 °C/min as the temperature-dependent dielectric measurement.

3 Results and discussion

3.1 Structural characterizations

Figure 1a shows the SEM image of a fresh fractured cross section of the Fe_2O_3 doped PMnS-PZN-PZT ceramics. It can be seen that the microstructure of the sample is generally dense and homogeneous, showing that the ceramics are well sintered. The average grain size is roughly estimated as about 2 μm. Besides, the cross-sectional morphology exhibits mixing of intergranular and transgranular fracture modes.

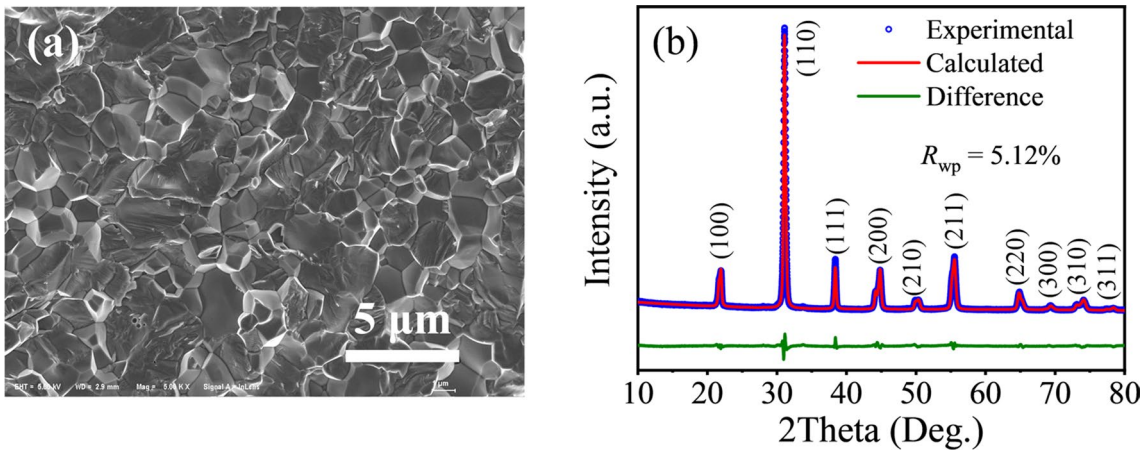

Fig. 1 Structural characterizations of Fe_2O_3 doped PMnS-PZN-PZT ceramics. **a** SEM image of a fresh fractured cross section; **b** XRD patterns and Rietveld refinement. The reflections are indexed in pesudocubic structure

The ratio of transgranular fracture is relatively high, suggesting a strong adhesion at the grain boundaries. According to the XRD patterns shown in Fig. 1b, the Fe_2O_3 doped PMnS-PZN-PZT ceramics exhibit a perovskite structure. Tetragonal distortion is present as evidenced by, for example, the (002)/(200) splitting. Rietveld refinement based on a tetragonal initial model (*P*4*mm*, ICSD-93554) acquires a good fit with an $R_{wp}=6.66\%$, which can be further improved to $R_{wp}=5.12\%$ by taking a rhombohedral structure (*R*3*c*, ICSD-93556) into the initial model, showing that the model of coexistence of tetragonal and rhombohedral phases is more reasonable than the model of single tetragonal phase. No peak splitting for the rhombohedral distortion could be observed, (e.g., the (111) reflection exhibit a single peak), and the reason is that the rhombohedral distortion is rather subtle. According to the refinement, the phase fractions are about 74.7% and 25.3% for the tetragonal and rhombohedral phases, respectively.

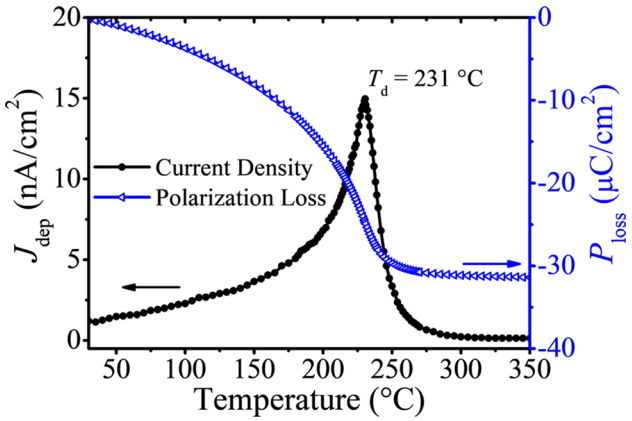

Fig. 2 Depolarization current density J_{dep} and polarization loss P_{loss} as functions of temperature. P_{loss} is calculated by integrating J_{dep} over time

3.2 TSDC and temperature-dependent dielectric property

TSDC measurement on a poled sample is used to determine the depolarization temperature [1]. Figure 2 shows the depolarization current density J_{dep} and the polarization loss P_{loss} plotted as functions of temperature, where the P_{loss} is calculated by integrating J_{dep} over time as

$$P_{loss} = -\int_{RT}^{T} J_{dep}\mathrm{d}t \quad (1)$$

From Fig. 2, a peak in J_{dep} is seen. This J_{dep} peak is corresponding to the steepest change in P_{loss}. By this peak, the depolarization temperature T_d of the Fe_2O_3 doped PMnS-PZN-PZT ceramics is determined to be 231 °C.

Figure 3a shows the temperature-dependent dielectric properties of Fe_2O_3 doped PMnS-PZN-PZT ceramics. The measurement was taken on an unpoled sample upon heating. A peak of ε_r is observed at $T_m=258$ °C, and no obvious frequency dependence of T_m can be found. For normal ferroelectrics, the dielectric peak is usually attributed to the transition from ferroelectric state to paraelectric state, and the dielectric maximum temperature T_m is usually very close to the depolarization temperature T_d because the depolarization is closely related to the ferroelectric-to-paraelectric transition [1]. In contrast, for the Fe_2O_3 doped PMnS-PZN-PZT ceramics, T_d is notably lower than T_m, showing that the depolarization may have nothing to do with the ferroelectric-to-paraelectric transition.

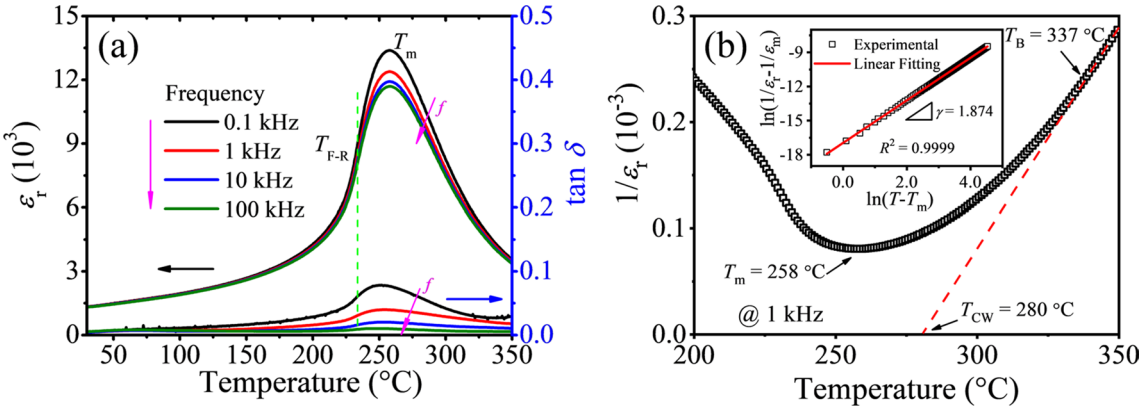

Fig. 3 Temperature-dependent dielectric properties of unpoled Fe_2O_3 doped PMnS-PZN-PZT ceramics. **a** Relative permittivity ε_r and loss factor tan δ; (b) the inverse of relative permittivity. The inset in **b** shows the fitting of modified Curie–Weiss law

The temperature-dependent dielectric measurement reveals that the Fe_2O_3 doped PMnS-PZN-PZT ceramics are similar to relaxors in some aspects of the dielectric behaviors. It can be seen from Fig. 3a that the relative permittivity ε_r shows an apparent dispersion with frequency around T_m, and the dielectric peak is obviously diffused. Figure 3b shows the inverse of relative permittivity at 1 kHz as a function of temperature. At the temperature above T_m, a deviation from Curie–Weiss law (Eq. (2)) is evident.

$$\frac{1}{\varepsilon_r} = \frac{T - T_{CW}}{C} \tag{2}$$

where C is the Curie constant and T_{CW} is the Curie–Weiss temperature. The onset temperature of the deviation from Curie–Weiss law is estimated to be about $T_B = 337$ °C (known as Burns temperature for relaxors [31]). To characterize the diffuseness of the relative permittivity peak, the modified Curie–Weiss law is used [32]

$$\frac{1}{\varepsilon_r} - \frac{1}{\varepsilon_m} = \frac{(T - T_m)^\gamma}{C'} \tag{3}$$

where ε_m is the maximum relative permittivity. The exponent γ indicates the degree of diffuseness of dielectric peak, with $1 \le \gamma \le 2$. The marginal values of $\gamma = 1$ and $\gamma = 2$ are corresponding to normal ferroelectric behavior and completely diffused dielectric peak, respectively. Generally, the diffused dielectric peak is a critical character of relaxors. For the Fe_2O_3 doped PMnS-PZN-PZT ceramic sample, as shown in the inset of Fig. 3b, the slope of $\ln(1/\varepsilon_r - 1/\varepsilon_m)$ versus $\ln(T - T_m)$ plot gives $\gamma = 1.847$, implying a highly relaxor-like behavior.

3.3 Identification of the transition from ferroelectric state to a "relaxor-like" state

Below T_m, we identify another characteristic temperature, denoted as T_{F-R} in Fig. 3a, which is defined by the temperature where ε_r, as well as tan δ, exhibits the fastest increases. However, the T_{F-R} is quite faint in the curve of temperature-dependent ε_r. To have a definite determination of T_{F-R}, the first derivative of ε_r with respect to temperature is calculated and plotted in Fig. 4a. A sharp peak can be observed in the first derivative of ε_r. By this peak, the T_{F-R} is determined to be 233 °C. At the temperature T_{F-R}, the rapid increases of ε_r and tan δ could be the smearing of discontinuous changes (see Fig. 3a), and probably an indication of a transition. Interestingly, the T_{F-R} does not change with frequency. More interestingly, the T_{F-R} from temperature-dependent dielectric measurement coincides well with the T_d from TSDC measurement. This coincidence is quite extraordinary, since the T_{F-R} and T_d are from two independent measurements.

Moreover, it is noted that the frequency dispersion of ε_r suddenly becomes pronounced when the temperature passes over T_{F-R} (see Fig. 3a). To quantify the frequency dispersion of ε_r, a parameter $\Delta\varepsilon_r$ is defined as

$$\Delta\varepsilon_r = \frac{\varepsilon_{r,0.1kHz} - \varepsilon_{r,100kHz}}{\varepsilon_{r,1kHz}} \tag{4}$$

Figure 4b shows $\Delta\varepsilon_r$ as a function of temperature. One can see that the $\Delta\varepsilon_r$ increases rapidly in the vicinity of T_{F-R}. This result is reminiscent of ferroelectric-to-relaxor transition. The rapid increases in ε_r and $\Delta\varepsilon_r$, accompanied with depolarization, around a frequency-independent temperature have previously been observed in many typical relaxor

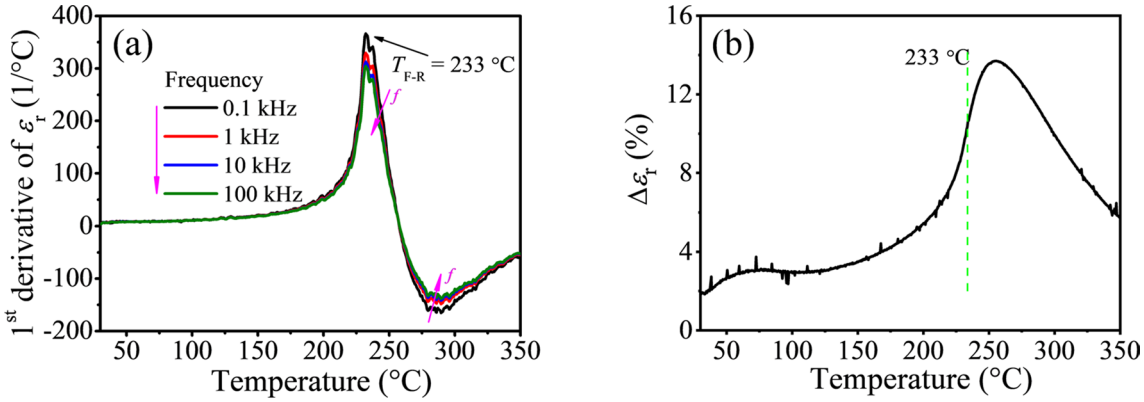

Fig. 4 Abrupt changes in dielectric properties around T_{F-R} for unpoled Fe_2O_3 doped PMnS-PZN-PZT ceramics. **a** The first derivative of relative permittivity with respect to temperature; **b** frequency dispersion in dielectric permittivity characterized by $\Delta\varepsilon_r$ as a function of temperature

ferroelectrics, such as PLZT [19, 33, 34], PMN/PZN-PZT [35, 36], BNT-BT/BKT [21, 37, 38], etc., and this characteristic temperature has been attributed to the ferroelectric-to-relaxor transition. For the Fe_2O_3 doped PMnS-PZN-PZT ceramic sample, in the view of these similarities, it is also reasonable to ascribe the T_{F-R} to a transition from the low-temperature ferroelectric state to some high-temperature "relaxor-like" state, in which the correlation of ferroelectric order is weakened. The exact nature of the relaxor-like state is remained unclear, which needed further investigations. In spite of the behaviors of Fe_2O_3 doped PMnS-PZN-PZT are highly relaxor-like, the ceramics could hardly be classified as relaxors, because the frequency dispersion of dielectric maximum is not observed.

More features of the anomaly around T_{F-R} are also noted. Figure 5a compares the temperature-dependent relative permittivity ε_r for the poled and unpoled samples. Although the poled sample possesses higher relative permittivity than that of the unpoled sample at room-temperature (probably due to the change of domain wall density and the domain texturing after poling), the relative permittivity above T_{F-R} for the poled and unpoled samples are approximately equal. The inset of Fig. 5a shows that the difference in ε_r between poled and unpoled samples, characterized by $(\varepsilon_{r,poled}/\varepsilon_{r,unpoled} - 1)$, suddenly diminishes around T_{F-R}. Another feature is that the temperature of the steepest increase in ε_r for the poled sample, which is determined to be 235 °C according to Fig. 5b, is almost the same as the T_{F-R} determined from the unpoled sample. Considering the poled sample is undoubtedly in ferroelectric state (see Ref. [25] for the saturated *P-E* hysteresis loop of the ceramics), the results from the poled sample further support that T_{F-R} is related to the transition from low-temperature ferroelectric state to high-temperature relaxor-like state.

As mentioned above, the dielectric anomalies at T_{F-R}, which have been ascribed to the transition from

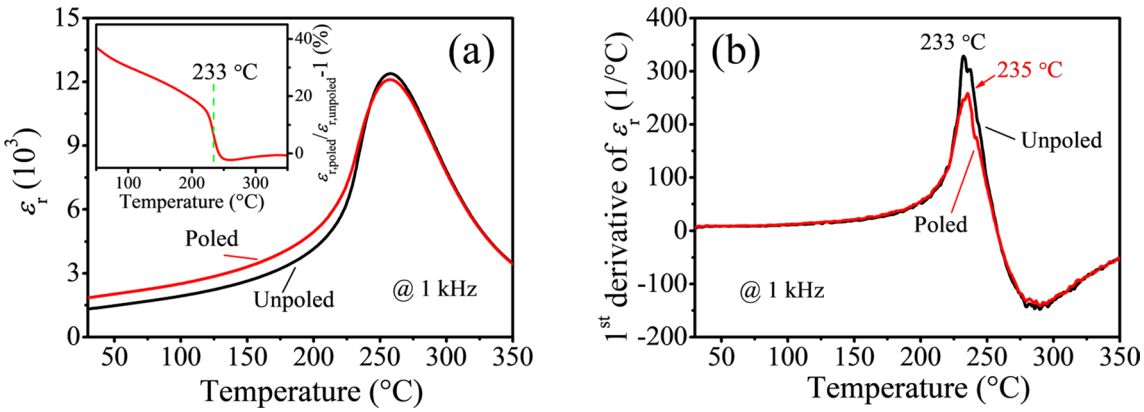

Fig. 5 Comparisons of temperature-dependent dielectric properties for poled and unpoled Fe_2O_3 doped PMnS-PZN-PZT ceramics. **a** Relative permittivity ε_r; **b** the first derivative of relative permittivity with respect to temperature. The inset in **a** shows the relative difference in relative permittivity between the poled and unpoled ceramics

low-temperature ferroelectric state to high-temperature relaxor-like state, can be detected on an unpoled sample. This means that the unpoled sample is also in ferroelectric state at room temperature. With this point, it is further speculated that the inverse transition may occur spontaneously during cooling. To confirm this, Fig. 6a compares the temperature-dependent ε_r measured upon heating and cooling, and Fig. 6b compares the first derivative of ε_r with respect to temperature. A peak in the cooling curve of first derivative of ε_r is observed at $T_{R\text{-}F} = 222$ °C. This peak reveals the spontaneous transition from high-temperature relaxor-like state to the low-temperature ferroelectric state [39–41]. In addition, $T_{R\text{-}F} < T_{F\text{-}R}$, which means that the transition between ferroelectric and relaxor-like states is first order in nature, with a transition hysteresis of about 11 °C.

3.4 Trace of small polarizable entities revealed by impedance spectra

More evidences for the high-temperature relaxor-like state are revealed by using the tool of complex impedance analysis. Figure 7a shows the imaginary part of complex modulus M'' spectra of Fe_2O_3 doped PMnS-PZN-PZT ceramics in the temperature range of 250 ~ 550 °C and the frequency range of 20 Hz ~ 300 kHz. Two sets of relaxation peaks can be seen: one is above 450 °C (denoted as "Peak A") and the other is below 350 °C (denoted as "Peak B"). With the increase of temperature, both peaks shift to higher frequency. Such a shifting trend implies that the characteristic frequency of Peak B should be higher than that of Peak A if the same temperature is considered.

To explore the origin of Peak A, the imaginary part of complex modulus M'', permittivity ε'' and impedance Z'' spectra are compared at 500 °C. As shown in Fig. 7b, the peak positions of M'' and Z'' overlap at about 400 Hz, whereas no obvious peak of ε'' is observed at the same frequency. Therefore, the Peak A is assigned to be the

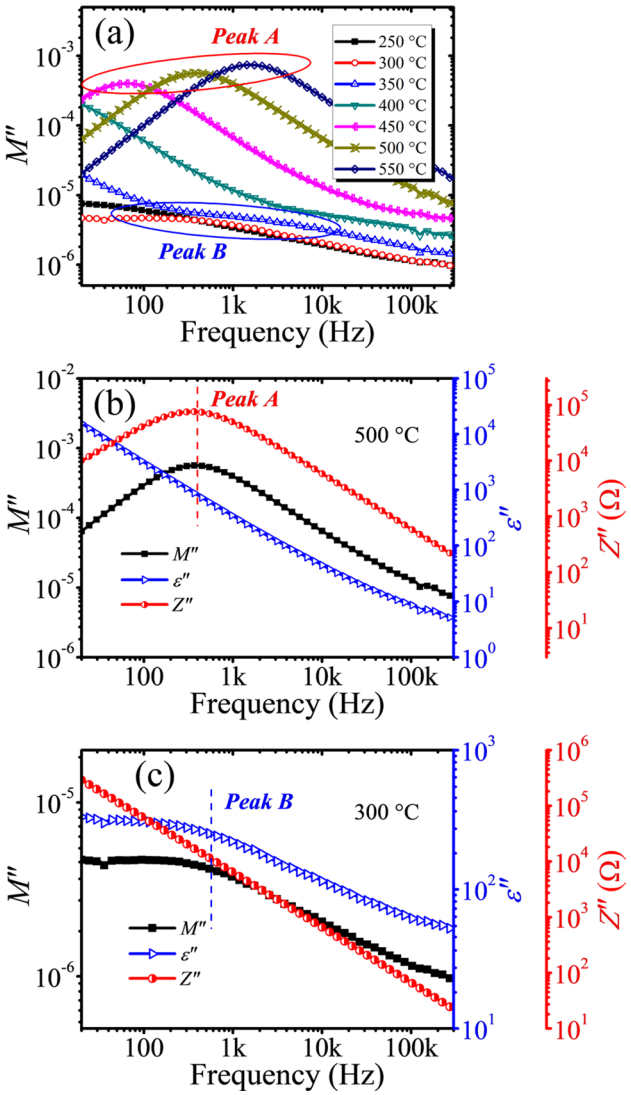

Fig. 7 Complex impedance spectra of Fe_2O_3 doped PMnS-PZN-PZT ceramics. **a** M'' spectra in the temperature range of 250 ~ 550 °C; comparisons of M'', ε'' and Z'' spectra at **b** 500 °C and **c** 300 °C

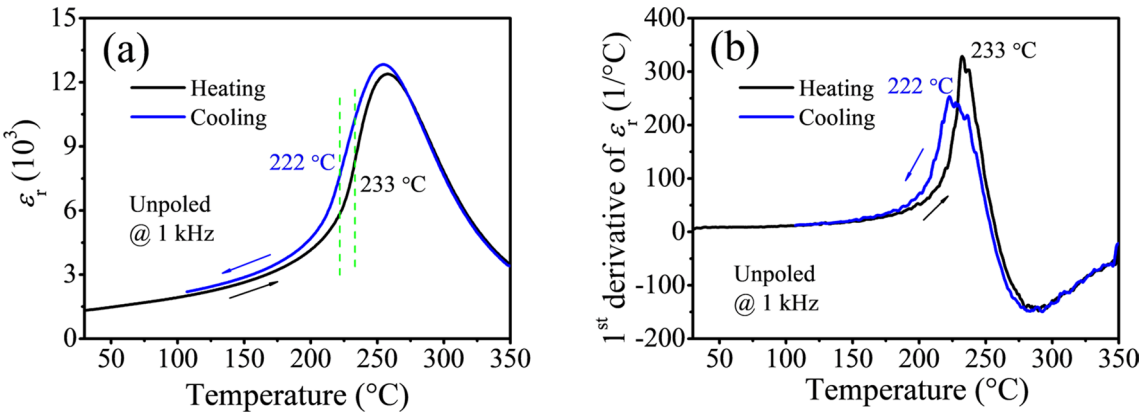

Fig. 6 Comparisons of temperature-dependent dielectric properties during heating and cooling processes for unpoled Fe_2O_3 doped PMnS-PZN-PZT ceramics. **a** Relative permittivity ε_r; **b** the first derivative of relative permittivity with respect to temperature

long-range conductivity [42, 43]. The relative permittivity estimated from the M'' peak ($2/M'' \approx 1700$) is similar to the value extrapolated from Curie–Weiss law ($\varepsilon_r \approx 1700$ at 500 °C, the Curie–Weiss fitting is shown Fig. 3b), which further confirms the assignment of Peak A. Generally, in polycrystalline ceramics, the difference in electrical properties between grains and grain boundaries leads to the separation of M'' and Z'' responses, with high-frequency M'' and Z'' peaks representing the response of grains and the low-frequency peaks representing the response of grain boundaries [44]. For the Fe_2O_3 doped PMnS-PZN-PZT, only one M'' and Z'' overlapped peak is observed, which means that the sample is electrically homogenous, and therefore the responses of grains and grain boundaries appear at approximately the same frequency.

As for the Peak B, Fig. 7c shows that the peaks of M'' and ε'' are overlapped, but no obvious peak of Z'' appears at the same frequency. The permittivity estimated from the Peak B ($2/M''_{max} \approx 15{,}000$) is much higher than that of the bulk value ($\varepsilon_r \approx 8000$, see Fig. 3a). In addition, the characteristic frequency of Peak B is higher than that of Peak A, and the Peak A has been assigned to be long-range conductivity. These features indicate that the Peak B is related to highly polarizable entities in small dimensions [42, 43]. These small-dimensional and highly polarizable entities may be originated from the disruption or weaken of ferroelectric order at $T_{F\text{-}R}$ and give rise to the relaxor-like behaviors of the ceramics, in analogous to the PNRs in typical relaxors [45]. To further clarify whether these polarized entities are indeed PNRs, more evidences are needed. Nevertheless, the appearance of Peak B confirms the existence of small polarizable entities in Fe_2O_3 doped PMnS-PZN-PZT ceramics.

The frequency dispersion of dielectric maximum temperature T_m is commonly observed for many relaxors, but the T_m of the Fe_2O_3 doped PMnS-PZN-PZT ceramics displays no frequency dispersion. We propose two possible reasons which could explain this phenomenon. The first reason is that the relaxor nature of Fe_2O_3 doped PMnS-PZN-PZT ceramics is somewhat faint, i.e., the contributions from the polarizable entities to the dielectric properties is very limited. From Figs. 7a and c, one can see that the Peak B is quite weak. The second reason is that when $T = T_m$, the relaxation frequency of the small polarizable entities is out of the frequency range (100 Hz ~ 100 kHz) of the temperature-dependent dielectric measurement. Wei et al. have demonstrated, for the typical relaxors Ba(Sn, Ti)O_3, that the frequency dispersion of T_m can only be observed when the experimental frequency covers the relaxation frequency of PNRs at the temperature around T_m [46]. As for the Fe_2O_3 doped PMnS-PZN-PZT ceramics, Fig. 8 shows the ε'' spectra in the temperature range of 250 ~ 350 °C. It can be seen that the Peak B has shifted below 100 Hz, the lower limit of the frequency range of temperature dielectric measurement, before the temperature decreases to T_m.

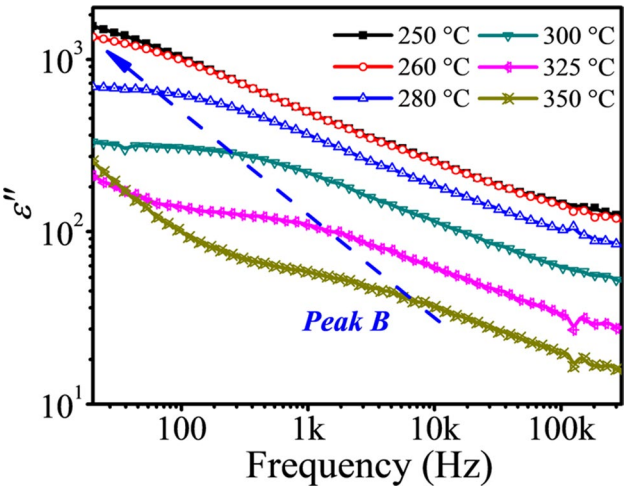

Fig. 8 ε'' spectra in the temperature range of 250 ~ 350 °C for Fe_2O_3 doped PMnS-PZN-PZT ceramics

3.5 Thermally induced transitions and depolarization

Based on the above analysis, we could outline the thermally induced transition and depolarization process of Fe_2O_3 doped PMnS-PZN-PZT ceramics. The thermally induced transition sequence is shown in Fig. 9. At room-temperature, the Fe_2O_3 doped PMnS-PZN-PZT is in ferroelectric state. With the increase of temperature, the transition from ferroelectric state to a relaxor-like state takes place at $T_{F\text{-}R} = 233$ °C. Above $T_{F\text{-}R}$, the ceramics are in relaxor-like state, and the small polarizable entities start to contribute to the dielectric responses, which give rise to the Peak B in the modulus spectra (Figs. 7a and c). When the temperature is further increased beyond Burns temperature $T_B = 337$ °C, the ceramics gradually evolve into paraelectric state. On cooling, the ceramics first evolve from paraelectric state into relaxor-like state around T_B, and then, the transition from relaxor-like state to ferroelectric state occurs spontaneously at $T_{R\text{-}F} = 222$ °C. Finally, the Fe_2O_3 doped PMnS-PZN-PZT is in ferroelectric state at room temperature. It is noted that the transition between ferroelectric and relaxor-like states is a first-order transition, with a thermal hysteresis of about 11 °C.

As for the depolarization, we have noted that the depolarization temperature T_d is notably lower than T_m, but coincident well with the temperature $T_{F\text{-}R}$ of the rapid increases in ε_r and $\Delta\varepsilon_r$. This behavior is quite in analogous to the typical relaxor ferroelectrics, where the depolarization is associated with ferroelectric-to-relaxor transition [19, 35, 38]. In this view, the depolarization of Fe_2O_3 doped PMnS-PZN-PZT

Fig. 9 Thermally induced transitions of Fe_2O_3 doped PMnS-PZN-PZT ceramics

ceramics is ascribed to the transition from low-temperature ferroelectric state to the high-temperature relaxor-like state, i.e., the reduction of correlation length of ferroelectric order, rather than the ferroelectric-to-paraelectric transition.

4 Conclusions

Thermally induced transitions and depolarization behavior of Fe_2O_3 doped PMnS-PZN-PZT ceramics are investigated. The first-order transition from low-temperature ferroelectric to high-temperature relaxor-like state takes place at $T_{F\text{-}R} = 233$ °C, and the inverse transition occurs spontaneously on cooling at $T_{R\text{-}F} = 222$ °C. In addition, the depolarization temperature T_d is determined to be 231 °C, which is notably lower than $T_m = 258$ °C but coincident well with $T_{F\text{-}R}$. The depolarization process is ascribed to the transition from low-temperature ferroelectric state to high-temperature relaxor-like state, i.e., the reduction in correlation length of ferroelectric order, rather than the ferroelectric-to-paraelectric transition. The present work also highlights the identification of $T_{F\text{-}R}$ by taking the first derivative of temperature-dependent dielectric permittivity. The rapid increase in dielectric permittivity in the vicinity of $T_{F\text{-}R}$ is likely to be a smearing of discontinuous change and therefore probably an indication of a transition. It would be interesting to check whether the coincidence of the depolarization temperature with the temperature of the fastest increase in dielectric permittivity is generally validated in other ferroelectric systems.

Acknowledgements This work is financially supported by the National Natural Science Foundation of China (No. 51572205, 51802093), the Post-Doctoral Innovation Research Project of Hubei Province (20201jb003), the Equipment Pre-Research Joint Fund of EDD and MOE (No. 6141A02033209) and the Fundamental Research Funds for the Central Universities (WUT: 2018III019, 2019IVA108, 2020III021).

References

1. E.-M. Anton, W. Jo, D. Damjanovic, J. Rödel, J. Appl. Phys. **110**, 094108 (2011)
2. C. Huang, K. Cai, Y. Wang, Y. Bai, D. Guo, J. Mater. Chem. C **6**, 1433 (2018)
3. H. Zhao, Y. Hou, M. Zheng, X. Yu, X. Yan, L. Li, M. Zhu, Mater. Lett. **236**, 633 (2019)
4. J. Rödel, K.G. Webber, R. Dittmer, W. Jo, M. Kimura, D. Damjanovic, J. Eur. Ceram. Soc. **35**, 1659 (2015)
5. S. Zhang, F. Yu, J. Am. Ceram. Soc. **94**, 3153 (2011)
6. J. Fialka, P. Benes, L. Michlovska, S. Klusacek, S. Pikula, P. Dohnal, Z. Havranek, J. Eur. Ceram. Soc. **36**, 2727 (2016)
7. R.E. Eitel, C.A. Randall, T.R. Shrout, P.W. Rehrig, W. Hackenberger, S.-E. Park, Jpn. J. Appl. Phys. **40**, 5999 (2001)
8. J. Zhang, Z. Pan, F.-F. Guo, W.-C. Liu, H. Ning, Y.B. Chen, M.-H. Lu, B. Yang, J. Chen, S.-T. Zhang, X. Xing, J. Rödel, W. Cao, Y.-F. Chen, Nat. Commun. **6**, 6615 (2015)
9. J. Ou-Yang, B. Zhu, Y. Zhang, S. Chen, X. Yang, W. Wei, Appl. Phys. A **118**, 1177 (2015)
10. T. Shinjiro, I. Masahiko, I. Hideji, Jpn. J. Appl. Phys. **36**, 3004 (1997)
11. S. Zhang, R. Xia, L. Lebrun, D. Anderson, T.R. Shrout, Mater. Lett. **59**, 3471 (2005)
12. K. Uchino, J.H. Zheng, Y.H. Chen, X.H. Du, J. Ryu, Y. Gao, S. Ural, S. Priya, S. Hirose, J. Mater. Sci. **41**, 217 (2006)
13. M. Hejazi, E. Taghaddos, E. Gurdal, K. Uchino, A. Safari, J. Am. Ceram. Soc. **97**, 3192 (2014)
14. J. Chen, Z. Hu, H. Shi, M. Li, S. Dong, J. Phys. D: Appl. Phys. **45**, 465303 (2012)
15. Z. Yao, H. Liu, H. Hao, M. Cao, J. Appl. Phys. **109**, 014105 (2011)
16. H. Law, P. Rossiter, G. Simon, J. Unsworth, J. Mater. Sci. **30**, 4901 (1995)
17. A. Bokov, Z.-G. Ye, J. Mater. Sci. **41**, 31 (2006)
18. V.V. Shvartsman, D.C. Lupascu, J. Am. Ceram. Soc. **95**, 1 (2012)
19. Y. Xi, C. Zhili, L.E. Cross, J. Appl. Phys. **54**, 3399 (1983)
20. D. Lin, K.W. Kwok, Appl. Phys. A **97**, 229 (2009)
21. W. Jo, S. Schaab, E. Sapper, L.A. Schmitt, H.J. Kleebe, A.J. Bell, J. Rödel, J. Appl. Phys. **110**, 074106 (2011)
22. E. Aksel, J.S. Forrester, B. Kowalski, M. Deluca, D. Damjanovic, J.L. Jones, Phys. Rev. B **85**, 024121 (2012)
23. Y. Liu, Z. Ling, Z. Zhuo, J. Appl. Phys. **124**, 164102 (2018)
24. J. Mao, J. Zhou, H. Zheng, H. Sun, W. Chen, J. Synth. Cryst. **39**, 72 (2010)
25. H. Zhang, J. Shen, J. Tian, J. Zhou, W. Chen, Ferroelectrics **491**, 15 (2016)
26. H. Zhang, J. Zhou, J. Shen, W. Jin, J. Zhou, W. Chen, Ferroelectrics **560**, 110 (2020)
27. J. Zhou, H. Sun, W. Chen, J. Chin. Ceram. Soc. **34**, 289 (2006)
28. J. Zhou, W. Peng, J. Guo, W. Chen, J. Chin. Ceram. Soc. **35**, 174 (2007)
29. J. Zhou, H. Sun, W. Chen, Piezoelect. Acoustoopt. **29**, 308 (2007)
30. L. Lutterotti, Nucl. Instrum. Methods Phys. Res., Sect. B **268**, 334 (2010)
31. G. Burns, F.H. Dacol, Solid State Commun. **48**, 853 (1983)
32. K. Uchino, S. Nomura, Ferroelectrics **44**, 55 (1982)
33. X. Dai, Z. Xu, D. Viehland, J. Appl. Phys. **79**, 1021 (1996)
34. X. Dai, Z. Xu, J.-F. Li, D. Viehland, J. Mater. Res. **11**, 618 (2011)
35. G. Du, R. Liang, J. Wang, L. Wang, W. Zhang, G. Wang, X. Dong, Ceram. Int. **39**, 9299 (2013)
36. R. Jiménez, B. Jiménez, J. Carreaud, J.M. Kiat, B. Dkhil, J. Holc, M. Kosec, M. Algueró, Phys. Rev. B **74**, 184106 (2006)
37. H. Zhang, J. Zhou, W. Chen, X. Yang, J. Shen, C. Wu, J. Electron. Mater. **46**, 6167 (2017)
38. S. Huband, P.A. Thomas, J. Appl. Phys. **121**, 184105 (2017)
39. M. Hagiwara, Y. Ehara, N. Novak, N.H. Khansur, A. Ayrikyan, K.G. Webber, S. Fujihara, Phys. Rev. B **96**, 014103 (2017)

40. N. Kumar, X. Shi, M. Hoffman, J. Eur. Ceram. Soc. **40**, 2323 (2020)
41. X. Dai, Z. Xu, D. Viehland, Philos. Mag. **70**, 33 (1994)
42. R. Gerhardt, J. Phys. Chem. Solids **55**, 1491 (1994)
43. J. Zang, M. Li, D.C. Sinclair, W. Jo, J. Rödel, J. Am. Ceram. Soc. **97**, 1523 (2014)
44. J.T.S. Irvine, D.C. Sinclair, A.R. West, Adv. Mater. **2**, 132 (1990)
45. A.A. Bokov, Z.-G. Ye, J. Adv. Dielectr. **02**, 1241010 (2012)
46. X. Wei, Y. Feng, X. Yao, Appl. Phys. Lett. **83**, 2031 (2003)